Electro-thermal Control of Modular Battery using Model Predictive Control with Control Projections

Electro-thermal Control of Modular Battery using Model Predictive Control with Control Projections ⋆

Faisal Altaf * **Bo Egardt** * **Lars Johannesson** *

* *Department of Signals and Systems, Chalmers University of Technology, Gothenburg, Sweden (e-mail: faisal.altaf@chalmers.se).*

Abstract: This paper proposes a novel model predictive control algorithm to achieve voltage regulation and simultaneous thermal and SOC balancing of a modular battery using limited future load information. The modular battery is based on multilevel converter (MLC), which provides a large redundancy in voltage synthesis and extra degree-of-freedom in control. The proposed algorithm is based on orthogonal decomposition of controller into two components, one for voltage control and the other for balancing control. The voltage control decisions are made using a simple minimum norm problem whereas the balancing control decisions are made in two stages. The first stage computes a balancing control policy based on an unconstrained LQ problem and the second stage enforces constraint on control actions via projection on a time-varying control constraint polytope. The control algorithm shows promising performance in a simulation study of a four cell modular battery. The performance and the simplicity of the control algorithm make it attractive for real-time implementation in large battery packs.

Keywords: Batteries, cell balancing, SOC balancing, thermal balancing, modular battery, multilevel converters (MLC), model predictive control (MPC).

1. INTRODUCTION

The battery-powered electrified vehicles (xEVs) have gained a lot of interest from academia as well as industry to improve fuel efficiency and reduce CO_2 emissions. The battery pack of xEVs is one of the most expensive, but a key component in the powertrain. Therefore, the battery lifetime is an important factor for the success of xEVs. The lithium-ion batteries, due to their relatively higher specific energy and long cycle-life, are currently emerging as one of the major alternative choices for future xEVs. However, like all other battery types, the ageing rate of each Li-ion cell in a battery pack is greatly affected by various factors like state-of-charge (SOC) level, depth-of-discharge (DOD), temperature, and c-rate etc as shown by Vetter et al. (2005); Wang et al. (2011); Bandhauer et al. (2011), and Groot (2014). In short, the cells in the string being stored or cycled at higher SOC-level, DOD and temperature age faster than those at lower SOC, DOD, and temperature. Therefore, thermal, SOC, and DOD imbalances in a battery pack may cause nonuniform ageing of cells. Another serious issue is that the cell imbalance and nonuniform ageing are tightly coupled, which may lead to a vicious cycle resulting in the premature end of battery life. In addition to nonuniform ageing, the SOC imbalance also has a detrimental impact on the total usable capacity of the battery, see review papers by Lu et al. (2013) and Altaf et al. (2014) for details. Thermal, SOC, and DOD imbalance is inevitable in battery packs of xEVs due to variations in cell parameters and operating conditions, see Dubarry et al. (2010); Mahamud and Park (2011). Thus, thermal and SOC balancer is very critical for optimal performance of automotive batteries. The SOC balancing can be achieved using various types of passive or active SOC balancers, see Gallardo-Lozano et al. (2014); Cao et al. (2008), whereas thermal balancing can potentially be achieved using reciprocating air-flow as proposed by Mahamud and Park (2011).

The notion of *simultaneous thermal and SOC balancing* using a single active balancing device was introduced in our previous work, see Altaf et al. (2012, 2013); Altaf (2014). A similar kind of conceptual study has also been carried out recently by Barreras et al. (2014). Thermal and SOC balancing are two tightly coupled and somewhat conflicting objectives, but it is possible to achieve both simultaneously in average sense subject to load variations and *surplus voltage* in a battery pack as argued by Altaf et al. (2014). In addition, it also requires a special balancing device that enables the non-uniform load scheduling of cells based on load predictions over a certain reasonable horizon. The *MLC-based modular battery* balancing system is a potential candidate for this purpose. The MLC, see Malinowski et al. (2010), consists of n cascaded power units (PUs), each containing a smaller battery unit and a full-bridge dc-dc converter, which enables bidirectional power flow from each battery module. The modular battery is reconfigurable to generate a range of terminal voltages. It also provides a large redundancy in the voltage synthesis, which gives extra degree-of-freedom in control.

The modular battery has multiple electro-thermal control objectives including thermal balancing, SOC balancing, and terminal voltage control. The electro-thermal control

⋆ The work was supported by the Chalmers Energy Initiative.

problem of the modular battery can be formulated and solved off-line as a constrained convex optimization problem, see Altaf et al. (2012, 2013); Altaf (2014). The solution is globally optimal if full information about complete future driving (i.e. future demand of load current and voltage over whole driving cycle) is accessible. However, in almost all vehicle applications, complete drive cycle is hardly known a priori, which makes the original problem infeasible for real world applications. Since it may still be possible to predict future driving over short horizons using, for example, a Markov Chain model, the natural alternative approach is to solve the problem in the model predictive control (MPC) framework as proposed by Altaf et al. (2015). In Altaf et al. (2015), a linear quadratic *model predictive control* scheme is proposed, which achieves the balancing objectives by using load forecast over a short prediction horizon. The control scheme is based on the *decomposition* of controller into two orthogonal components, one for voltage control and the other for balancing control. The *voltage control problem* is a simple minimum norm problem, whereas the *balancing problem* is formulated and solved as a *control-constrained LQ MPC* problem.

This paper is an extension of Altaf et al. (2015). The main purpose is to devise an alternative control algorithm, which uses the same controller structure as proposed in Altaf et al. (2015), but solves the *balancing control problem* using a simpler approach instead of solving control-constrained LQ problem at each step of MPC. The main idea is to solve the control-constrained balancing problem in two stages at each step. In the first stage, unconstrained optimal balancing control decisions are made based on *unconstrained LQ control policy* and in the second stage the control constraint is handled via *projection* of unconstrained controls on control constraint set (polytope). This *control scheme based on control projections* adds more insight into properties of MLC-based thermal and SOC balancer and offers some nice interpretations. This new method (so-called *projected LQ*) of solving balancing problem is fast and can be easily implemented online as it is based on simple Riccati recursion and projections, which are rarely needed if the SOC imbalance and/or the load demand is not too high.

The new control scheme is evaluated in a simulation study for *Standard ARTEMIS Rural* drive cycle. The study is focussed on an air-cooled modular battery consisting of only four series-connected modules for illustration purpose. In order to analyze the effectiveness of the control scheme, the cells are assumed to have significant differences in their resistances, capacities, and initial SOCs. The load on the modular battery is assumed to be three-phase electric drive of Toyota Prius PHEV running in pure EV mode.

The paper is organized as follows. Section 2 gives an overview of MLC-based modular battery. The electro-thermal state-space model and the control algorithm based on LQ MPC scheme are presented in sections 3 and 4 respectively. The simulation results are discussed in section 5 and conclusions are drawn in section 6.

2. MLC-BASED MODULAR BATTERY: OVERVIEW

The (cascaded h-bridge) MLC-based modular battery, supplying voltage $v_L(t) \in [0, v_{L\max}] \subseteq \mathbb{R}_+$ to a variable

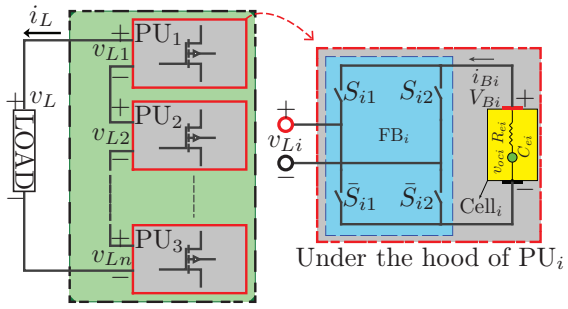

Fig. 1. MLC-based n-cell modular battery in green box.

load (three-phase ac drive of xEV) with current demand $i_L(t) \in [i_{L\min}, i_{L\max}] \subseteq \mathbb{R}$, is shown in Figure 1. The MLC consists of n series-connected PUs, each containing a full-bridge (FB) and an isolated Cell$_i$ represented by open-circuit voltage source (OCV) v_{oci} in series with resistance R_{ei}. This modular structure enables the distribution of a single large high-voltage battery into n smaller low-voltage *units* (cells). We can generate three different discrete levels of output voltage $v_{Li}(t) \in \{-V_{Bi}, 0, +V_{Bi}\}$ from each PU$_i$, allowing four quadrant operation in i_L–v_{Li} plane, which enables *control of bidirectional power flow* from each cell.

The FB switches are commonly operated using a high frequency switching function $s_i(t)$, which is generated by a modulator using a certain pulse-width modulation (PWM) scheme. In this paper, we are only interested in controlling the average behavior of a switched modular battery during each switching period $T_{\rm sw}$ of $s_i(t)$. Therefore, assuming fast PWM operation of switches, we define duty-cycle,

$$u_i(t) := \frac{1}{T_{\rm sw}} \int_{t-T_{\rm sw}}^{t} s_i(\tau) \mathrm{d}\tau, \tag{1}$$

of each PU$_i$. Note that $u_i(t) \in [-1, 1]$, where negative value implies $v_{Li}(t) < 0$ and positive value implies $v_{Li}(t) \geq 0$. In this study, we assume that the controller is positively constrained i.e. $u_i(t) \in [0, 1]$ (so-called *unipolar control scheme*). This scheme does not allow polarity inversion of any cell in the string, which simply implies that at any time instant, either all cells are charging (for $i_L(t) < 0$) or all are discharging (for $i_L(t) > 0$).

The *average inputs* $(i_{Bi}(t), V_{Bi}(t))$ and *average outputs* $(i_L(t), v_{Li}(t))$ of ideal FB$_i$ are linearly related through unipolar duty cycle $u_i(t) \in [0, 1]$ as follows

$$i_{Bi}(t) = i_L(t) u_i(t), \quad v_{Li}(t) = V_{Bi}^{\rm on}(t) u_i(t), \tag{2}$$

where $i_{Bi}(t)$ is the current through each Cell$_i$, $v_{Li}(t)$ is the voltage output from each PU$_i$, $i_L(t)$ is the load current through the output terminals of the modular battery, and

$$V_{Bi}^{\rm on}(t) = v_{oci} - i_L(t) R_{ei} \tag{3}$$

is the terminal voltage of Cell$_i$ during its so-called *ON period* (i.e. the time interval in a switching period $T_{\rm sw}$ during which Cell$_i$ is connected in series electrical path and delivering/absorbing power). The terminal voltage and power of the modular battery are given by

$$v_L(t) = \sum_{i=1}^{n} v_{Li}(t), \quad P_L(t) = \sum_{i=1}^{n} P_{Li}(t), \tag{4}$$

respectively, where $P_{Li}(t) = v_{Li}(t) i_L(t)$ is the power output from each PU$_i$, see Altaf et al. (2012) for details on averaging of all switched waveforms involved here.

3. STATE-SPACE ELECTRO-THERMAL MODEL

The electro-thermal model of an air-cooled modular battery consisting of n series-connected modules with *ideal switches* is presented in this section. The electrical behavior of cells is studied using the *simple cell model*, see Hu et al. (2012), which for each cell is based on internal resistance (R_{ei}), in series with OCV (v_{oci}). The v_{oci} of all cells is assumed constant in this study. This approximation is somewhat justified for certain types of lithium-ion cells (for example $LiFePO_4$/graphite (LFP)) if we assume battery operation in a typical SOC window of 20% to 90%. The thermal behavior of air-cooled battery is modeled using lumped capacitance and flow network modeling approach, see Mahamud and Park (2011); Lin et al. (2013a,b). The model considers only cell casing temperature with constant coolant temperature and speed at inlet. All internal parameters of cells are assumed constant i.e. they are not function of time, temperature and SOC. For more modeling details, see Altaf et al. (2012, 2013), and Altaf (2014).

3.1 Electro-thermal Model of One Cell

The electro-thermal model of any Cell_i inside modular battery for a given load current $i_L(t)$ is given by

$$\dot{\xi}_i(t) = -\frac{1}{3600 C_{ei}} i_L(t) u_i(t), \tag{5a}$$

$$\dot{T}_{si}(t) = \sum_{j=1}^{i} a_{tij} T_{sj}(t) + \frac{R_{ei}}{C_{si}} i_L^2(t) u_i(t) + w_{ti} T_{f0}, \tag{5b}$$

$$v_{Li}(t) = d_{vi}(t) u_i(t), \tag{5c}$$

where a_{tij} and w_{ti} are thermal circuit parameters given by

$$a_{tij} = \left(\frac{\prod_{k=(j+1)}^{(i-1)} \beta_k}{\prod_{k=j}^{(i-1)} \alpha_k} \right) a_{si}, \ \forall i > j, \ a_{tij} = 0, \ \forall i < j \tag{6a}$$

$$a_{tij} = -a_{si}, \ \ \forall i = j \geq 1, \ w_{ti} = -\sum_{j=1}^{i} a_{tij} \ \forall i \geq 1 \tag{6b}$$

for coolant flow from Cell_1 towards Cell_n, C_{ei} is the practical charge capacity of Cell_i, R_{ei} is the internal resistance and $C_{si}\,[JK^{-1}]$ is the heat capacity of Cell_i. Temperature, $T_{si}(t)$, and normalized SOC, $\xi_i(t)$, are states, T_{f0} is the given constant inlet fluid temperature, $v_{Li}(t)$ is the voltage output of PU_i in response to the input current $i_{Bi}(t)$, and $d_{vi}(t) = V_{Bi}^{\text{on}}(t)$, defined in (3), is a time-varying feed-through gain from control input $u_i(t)$ to the voltage output $v_{Li}(t)$. All other parameters are defined in Table 1.

3.2 Electro-thermal Model of Modular Battery

Using (5a)–(5c) as basic building block and treating T_{f0} as a dummy state, the continuous-time (CT) electro-thermal model of a n-cell modular battery is given by the following standard linear time-varying (LTV) state-space system

$$\dot{x}(t) = Ax(t) + B(i_L(t))u(t), \tag{7a}$$

$$y(t) = Cx(t) + D(i_L(t))u(t). \tag{7b}$$

Here $x(t) = \left[\xi^{\mathrm{T}}(t) \ \vartheta^{\mathrm{T}}(t)\right]^{\mathrm{T}} \in \mathbb{R}^{2n+1}$ is the complete state vector, $\xi(t) = [\xi_1 \ \cdots \ \xi_n]^{\mathrm{T}} \in \mathbb{R}^n$ is a vector of SOCs, $\vartheta(t) = \left[T_s^{\mathrm{T}}(t) \ T_{f0}\right]^{\mathrm{T}} \in \mathbb{R}^{n+1}$ is an augmented thermal state with $T_s(t) = [T_{s1} \ \cdots \ T_{sn}]^{\mathrm{T}} \in \mathbb{R}^n$, $u(t) = [u_1 \ \cdots \ u_n]^{\mathrm{T}} \in \mathbb{R}^n$ is the unipolar control input vector, $y(t) = \left[\vartheta^{\mathrm{T}}(t) \ v_L(t)\right]^{\mathrm{T}} \in \mathbb{R}^{n+2}$ is the output vector, and

$$A = \begin{bmatrix} A_E & 0 \\ 0 & A_\vartheta \end{bmatrix}, \ B(i_L(t)) = \begin{bmatrix} B_E i_L \\ B_\vartheta i_L^2 \end{bmatrix},$$

are constant system and time-varying input matrices respectively. The corresponding state-space matrices of electrical and thermal subsystem are given by

$$A_E = 0_{n\times n}, \ B_E = -\frac{1}{3600}\text{diag}\,(b_{e1}, \cdots, b_{en}) \in \mathbb{R}^{n\times n},$$

$$A_\vartheta = \begin{bmatrix} A_T & W_T \\ 0_n^{\mathrm{T}} & 0 \end{bmatrix}, \ \ B_\vartheta = \begin{bmatrix} B_T \\ 0_n^{\mathrm{T}} \end{bmatrix},$$

$$B_T = \text{diag}\,(b_{t1}, \cdots, b_{tn}) \in \mathbb{R}^{n\times n},$$

$$W_T = [w_{t1} \ \cdots \ w_{tn}]^{\mathrm{T}} \in \mathbb{R}^n,$$

where $A_T \in \mathbb{R}^{n\times n}$ is a lower triangular constant thermal subsystem matrix with coefficients a_{tij} given by (6a) and (6b), and the coefficient $b_{ei} = \frac{1}{C_{ei}}$ and $b_{ti} = \frac{R_{ei}}{C_{si}}$. The constant output matrix C and time-varying feed-through matrix $D(t)$ are respectively defined as follows

$$C = \begin{bmatrix} 0 & I_{n+1} \\ 0_n^{\mathrm{T}} & 0_{n+1}^{\mathrm{T}} \end{bmatrix}, \ D(i_L(t)) = \begin{bmatrix} 0 \\ D_v(t) \end{bmatrix},$$

where

$$D_v(t) = [d_{v1}(t) \ \cdots \ d_{vn}(t)] \in \mathbb{R}^{1\times n}, \tag{8}$$

is a direct feedthrough gain from control vector $u(t)$ to the total voltage output $v_L(t)$. From the output equation (7b), it is easy to see that $v_L(t)$ is simply given by

$$v_L(t) = \sum_{i=1}^{n} v_{Li} = \sum_{i=1}^{n} d_{vi}(t) u_i = D_v(t) u(t). \tag{9}$$

The discrete-time (DT) state-space model is given by

$$x(k+1) = A_d x(k) + B_d(i_L(k))u(k), \tag{10a}$$

$$y(k) = Cx(k) + D(i_L(k))u(k), \tag{10b}$$

where A_d and $B_d(k)$ are obtained using Euler approximation assuming $i_L(k)$ to be constant during each sampling interval $[kh, (k+1)h]$ where h is a sampling step size.

3.3 Control Constraint Set

The unipolar control scheme imposes control constraint $u_i(k) \in [0, 1]$ for each Cell_i. Therefore, the control constraint set of n-cell modular battery is given by

$$\mathcal{U} = \{u(k) | H_u u \leq h_u, \ \forall k\}, \tag{11}$$

for suitably defined H_u and h_u.

Table 1. Definition of Cell/Coolant Parameters

Parameters	**Expression**	**Units**
OCV of Cell_i	v_{oci}	V
Electrical Resistance	R_{ei}	Ω
Charge Capacity	C_{ei}	Ah
Thermal Resistance	R_{ui}	KW^{-1}
Air Density	ρ_f	$kg\,m^{-3}$
Air Specific Heat Capacity	c_{pf}	$JK^{-1}kg^{-1}$
Air Volumetric Flow Rate	$\dot{V}_f$	$m^3 s^{-1}$
Air Thermal Conductance	$c_f = \rho_f c_{pf} \dot{V}_f$	WK^{-1}
Temperature Coeff.	$a_{si} = (C_{si} R_{ui})^{-1}$	s^{-1}
Thermal Coupling Coeff.	$\alpha_i = R_{ui} c_f$	Unitless
Thermal Coupling Coeff.	$\beta_i = -1 + \alpha_i$	Unitless

4. CONTROL PROBLEM FORMULATION

The electro-thermal control objectives include simultaneous thermal and SOC balancing as well as terminal voltage control of modular battery. Assuming that the full future load demand is available, we may impose zone and terminal constraints on SOC and temperature deviations, formulate the problem as a *state and control constrained convex optimization problem* over whole driving horizon N_d, and then solve it to get optimal control trajectory $\{u(k)\}_{k=1}^{N_d}$ in one shot. However, this assumption is quite unrealistic especially in xEVs.

Therefore, Altaf et al. (2015) proposed a control strategy based on LQ MPC scheme to solve the original problem using limited future driving information (i.e. horizon $N \ll N_d$). The proposed scheme prioritizes the *load voltage regulation* (supply = demand). Thermal and SOC balancing are treated as secondary objectives, which are achieved by optimally using any redundancy available in the modular battery after meeting power demand. The control strategy is mainly developed based on the decomposition of *total controller* into two *orthogonal components* as follows

$$u(k) = u_v(k) + u_b(k) \in \mathcal{U}, \tag{12}$$

where control $u_v(k) \in \mathcal{N}(D_v(k))^\perp$ is for *voltage control* and $u_b(k) \in \mathcal{N}(D_v(k))$ is for *balancing control* where $\mathcal{N}(D_v(k))$ is the nullspace of $D_v(k)$ and $\mathcal{N}(D_v(k))^\perp$ is the orthogonal complement of $\mathcal{N}(D_v(k))$. The time-varying nullspace of $D_v(k)$ is a hyperplane in $\mathbb{R}^n$ given by

$$\mathcal{N}(D_v) = \{u(k) | D_v(k)u(k) = 0\} = \mathcal{R}(V_\mathrm{n}) \subseteq \mathbb{R}^n, \tag{13}$$

where $\mathcal{R}(V_\mathrm{n})$ is the range-space of null-space basis matrix

$$V_\mathrm{n}(k) = [v_{\mathrm{n},1}(k) \ \cdots \ v_{\mathrm{n},n-1}(k)] \in \mathbb{R}^{n \times n-1},$$

which contains parameterized orthonormal basis vectors $v_{\mathrm{n},i}(k) \in \mathbb{R}^n$ of null-space. A particular choice of V_n, obtained using MATLAB® Symbolic Toolbox, is given by

$$V_\mathrm{n}(k) = \begin{bmatrix} V_\mathrm{n}'(k) \\ I_{n-1} \end{bmatrix}, \tag{14}$$

where $V_\mathrm{n}'(k) = -\begin{bmatrix} \frac{d_{v2}(k)}{d_{v1}(k)} & \cdots & \frac{d_{vn}(k)}{d_{v1}(k)} \end{bmatrix} \in \mathbb{R}^{1 \times (n-1)}$ is a row vector with elements $d_{vi}(k) = v_{oci} - i_L(k)R_{ei}$. The proposed orthogonal decomposition guarantees the voltage constraint satisfaction while giving the possibility of simultaneous balancing. The *voltage control problem* is a minimum norm problem, whereas the *balancing problem* is formulated as a *control-constrained LQ MPC* problem.

In this study, we simplify the balancing controller even further. The aim is to achieve $u(k) \in \mathcal{U}$ using a simpler approach instead of solving control constrained LQ problem at each step of MPC. We propose to compute the balancing control *policy* $u_b(k)$ in receding horizon fashion based on *unconstrained LQ* problem whereas control constraint, if violated, is handled later via projection of unconstrained control actions on control constraint set. In the following, we first summarize the voltage control problem and then in section 4.2 we formulate and solve the alternative balancing control problem in detail.

4.1 Voltage Controller: Least-norm Problem

The control $u_v(k)$ at each time instant can be computed by directly solving the output equation (9) to satisfy $v_L(k) = v_{Ld}(k)$ for any given load current demand $i_L(k)$. However, $D_v(k)u_v(k) = v_{Ld}(k)$ has infinite solutions due to nonempty nullspace of $D_v(k)$, which is an n–dimensional row vector. A unique solution $u_v \in \mathcal{N}(D_v)^\perp$ is simply given by the following least norm problem

$$\begin{aligned} \text{minimize} \quad & \|u_v(k)\| \\ \text{subject to} \quad & D_v(k)u_v(k) = v_{Ld}(k), \\ & u_v(k) \in \mathcal{U}, \end{aligned} \tag{P-I}$$

which is feasible for load demands $i_L(t) \in [i_{L\min}, i_{L\max}]$ and $v_{Ld}(t) \in [0, v_{Ld\max}]$ with appropriately defined limits $i_{L\min}, i_{L\max}$, and $v_{Ld\max}$. Note that $u_v(k)$ is a feedforward controller, which uses information only about demanded load data $v_{Ld}(k)$ and $i_L(k)$, given at each time instant.

4.2 Balancing Controller: LQ MPC with Projections

The balancing control objective is to find a *control policy* $u_b(k)$ that minimizes SOC and temperature deviations among cells without increasing average battery temperature relative to that of unbalanced battery, disturbing voltage $v_L(k)$, and violating the constraint $u(k) \in \mathcal{U}$. The null-space $\mathcal{N}(D_v)$ provides the extra degree-of-freedom, which can be used to tweak temperature and SOC of cells while exactly satisfying the voltage demand. Therefore, after computing the voltage control decision $u_v(k)$, we can appropriately choose balancing control $u_b(k) \in \mathcal{N}(D_v)$ to achieve thermal and SOC balancing objectives simultaneously. The balancing control can be computed by the linear combination of the basis vectors of nullspace as follows

$$u_b(k) = \sum_{i=1}^{n-1} \rho_{bi}(k) v_{\mathrm{n},i}(k) = V_\mathrm{n}(k)\rho_b(k) \in \mathcal{U}_b(k), \tag{15}$$

where $V_\mathrm{n}(k)$ is given by (14) and $\rho_b(k) \in \mathbb{R}^{n-1}$ are coefficients of null-space basis vectors, and $\mathcal{U}_b(k)$, discussed below, is a time-varying set of feasible $u_b(k)$. Note that the problem of finding optimal $u_b(k)$ is now equivalent to finding optimal control coefficients $\rho_b(k)$. We solve the constrained balancing control problem in *two stages*:

1. *Unconstrained LQ Control Problem:* Firstly, we formulate the balancing control problem on standard LQ form to find unconstrained policy $u_{b,\mathrm{lq}}(k) = K_{u_b}(k)x(k)$. The control policy $u_{b,\mathrm{lq}}(k)$ is computed indirectly i.e. we first solve the LQ problem in terms of $\rho_b(k)$ and then, using (15), we get $u_{b,\mathrm{lq}}(k)$.
2. *Constrained Control via Projection:* Secondly, we compute constrained control action by projecting $u_{b,\mathrm{lq}}(k)$ on the constraint set $\mathcal{U}_b(k)$.

In the following, we discuss all the important ingredients involved in these two stages.

Balancing Control Constraint (Truncated Null-Space): The null-space coefficients $\rho_b(k)$ must be chosen such that the total control $u(k) \in \mathcal{U}$. This means we can only choose balancing control from so-called truncated null-space $\mathcal{U}_b \subseteq \mathcal{N}$. In simple words, $\mathcal{U}_b$ defines the set of feasible balancing controls at each time instant. The truncated null-space $\mathcal{U}_b$ can be easily represented in terms of constraint on coefficients $\rho_b(k)$. This is achieved by mapping control constraint set $\mathcal{U}$ and voltage control $u_v(k)$ on the coefficient space as follows. From (12), it is straightforward to see that $u_b(k)$ must satisfy the following time-varying constraint

$$u_{\min} - u_v(k) \le u_b(k) = V_{\rm n}(k)\rho_b(k) \le u_{\max} - u_v(k), \quad (16)$$

which can be represented by the following convex set

$$\mathcal{P}_b(k) = \{\rho_b(k) \,|\, H_{\rho_b}(k)\rho_b(k) \le b_{\rho_b}(k)\} \subseteq \mathbb{R}^{n-1}, \quad (17)$$

in variables $\rho_b(k)$ where $u_{\min} = 0_n$, $u_{\max} = 1_n$, and

$$H_{\rho_b}(k) = \begin{bmatrix} -V_{\rm n}(k) \\ V_{\rm n}(k) \end{bmatrix}, \quad b_{\rho_b}(k) = \begin{bmatrix} -b_{\rho_b,\min}(k) \\ b_{\rho_b,\max}(k) \end{bmatrix} \quad (18)$$

are time-varying inequality constraint matrices where $V_{\rm n}(k)$ is defined in (14) and

$$b_{\rho_b,\min}(k) = u_{\min} - u_v(k),\ b_{\rho_b,\max}(k) = u_{\max} - u_v(k) \quad (19)$$

define time-varying lower and upper boundaries on null-space $\mathcal{N}(D_v)$ as well as its coefficients $\rho_b(k)$. Now we can define balancing control constraint set as follows

$$\mathcal{U}_b(k) = \{u_b(k) = V_{\rm n}(k)\rho_b(k) \,|\, \rho_b(k) \in \mathcal{P}_b(k)\} \subseteq \mathbb{R}^n. \quad (20)$$

Note that $\mathcal{U}_b(k)$ is a polytope whose boundaries are function of load demands (v_{Ld} and i_L). For example, for a 4-cell battery with $v_L = 9.25\,V$, Fig. 3(a) shows projection of $\mathcal{U}_b(i_L)$ on 2-dimensional plane for various values of i_L.

Balancing Objective Function: The standard quadratic objective function given by

$$\begin{aligned} J(x(k), \rho_b(k:k+N'-1)) &= \|x(k+N')\|^2_{\bar{P}_x} \\ &+ \sum_{l=0}^{N'-1} \left[\|x(k+l)\|^2_{\bar{Q}_x} + \|\rho_b(k+l)\|^2_{R_{\rho_b}} \right], \end{aligned} \quad (21)$$

$$\text{with } N' = \begin{cases} N, & \text{if } k \le N_d - N + 1, \\ N_d - k + 1, & \text{otherwise} \end{cases} \quad (22)$$

over prediction horizon N achieves the desired balancing goal by adding quadratic costs $q_E \left(\xi_i(l) - \bar{\xi}(l)\right)^2$ and $q_T \left(T_{si}(l) - \bar{T}_s(l)\right)^2 + q_{\bar{T}} \bar{T}_s^2(l)$ for all cells at each time instant l inside prediction phase where $\bar{\xi}(l) = \frac{1}{n} 1_n^{\rm T} \xi(l)$ and $\bar{T}_s(l) = \frac{1}{n} 1_n^{\rm T} T_s(l)$ are *mean SOC* and *mean temperature* of the modular battery respectively. The penalty weight matrices for complete objective function are given by

$$\bar{Q}_x = \text{blkdiag}\left(\gamma_1 \bar{Q}_E, \gamma_2 \bar{Q}_T + \gamma_3 \bar{Q}_{\bar{T}}, 0\right), \quad (23)$$

$$\bar{P}_x = \text{blkdiag}\left(\gamma_1 \bar{P}_E, \gamma_2 \bar{P}_T + \gamma_3 \bar{P}_{\bar{T}}, 0\right), \quad (24)$$

$$R_{\rho_b}(k) = \gamma_4 V_n^{\rm T}(i_L(k)) R_{u_b} V_{\rm n}(i_L(k)), \quad (25)$$

where $\gamma_i \ge 0$ are trade-off weights, which signify the relative importance of each objective, $R_{\rho_b}(k)$ and R_{u_b} are time-varying penalty weights for $\rho_b(k)$ and $u_b(k)$ respectively, and

$$\bar{Q}_E = \frac{1}{2} \bar{M}_2^{\rm T} Q_E \bar{M}_2, \ \bar{P}_E = \frac{1}{2} \bar{M}_2^{\rm T} P_E \bar{M}_2, \quad (26a)$$

$$\bar{Q}_T = \frac{1}{2} \bar{M}_2^{\rm T} Q_T \bar{M}_2, \ \bar{P}_T = \frac{1}{2} \bar{M}_2^{\rm T} P_T \bar{M}_2, \quad (26b)$$

$$\bar{Q}_{\bar{T}} = \frac{1}{n} q_{\bar{t}} M_2, \qquad \bar{P}_{\bar{T}} = \frac{1}{n} p_{\bar{t}} M_2. \quad (26c)$$

are running and terminal penalty weights for SOC and temperature where $\bar{M}_2 = I_n - M_2$ with $M_2 = \frac{1}{n} 1_{n\times n}$ maps each cell SOC and temperature to their corresponding deviations from *mean SOC and temperature* (defined above) of modular battery. Note that the weights γ_i are chosen such that $\sum_i^4 \gamma_i = 1$, to achieve desired trade-off between temperature and SOC balancing performance.

Unconstrained LQ Control Problem: The optimal coefficient vector $\rho_b(k)$ for the balancing control $u_b(k)$ is computed at each time step $k \in \{0, \cdots, N_d\}$ by solving the following standard unconstrained LQ problem in a receding horizon fashion.

$$\begin{aligned} &\text{minimize} \quad J(x(k), \rho_b(k:k+N'-1)) \\ &\text{subject to} \\ &x(k+l+1) = A_d x(k+l) + \bar{B}_d(k+l)\rho_b(k+l), \\ &\forall l = \{0, \cdots, N'-1\}, \end{aligned} \quad \text{(P-II)}$$

with optimization variables $x(l)$ and $\rho_b(l)$ where l, as defined above, is the time index for the prediction phase of MPC, N_d is the driving horizon, and $N' \ll N_d$ as defined in (22) is the prediction horizon. Note that, by substituting $u(k)$ with $u_b(k) = V_{\rm n}(k)\rho_b(k)$ as a control variable in (10a), we get the system dynamics in terms of new control variable $\rho_b(k)$ as shown in (P-II) above where

$$\bar{B}_d(k+l) = B_d(i_L(k+l)) \cdot V_{\rm n}(i_L(k+l)).$$

The problem (P-II) is an unconstrained LQ control problem. The *unconstrained optimal control policy* is given by

$$\rho_{\rm lq}(k) = K_{\rho_b}(k) x(k), \quad (27)$$

$$u_{b,{\rm lq}}(k) = K_{u_b}(k) x(k),\ K_{u_b}(k) = V_{\rm n}(k) K_{\rho_b}(k), \quad (28)$$

$$u_{\rm lq}(k) = u_v(k) + u_{b,{\rm lq}}(k), \quad (29)$$

where $K_{\rho_b}(k)$ and $K_{u_b}(k)$ are control gain matrices obtained using standard time-varying Riccati equation. Note that the control policy $u_{b,{\rm lq}}$ uses feedback about battery state x as well as feedforward knowledge about i_L and voltage control u_v, to achieve balancing objectives.

Constrained Control via Projection on $\mathcal{U}_b(k)$: The control actions $u_{\rm lq}(k)$ based on unconstrained balancing control policy (28) can violate the constraint $\mathcal{U}$ especially in cases where we have large thermal and SOC deviations and high load demands. The control $u(k) \in \mathcal{U}$ respecting the voltage constraint is guaranteed if $u_b(k) \in \mathcal{U}_b(k)$. Therefore, we propose to project $u_{b,{\rm lq}}(k)$ on the polytope $\mathcal{U}_b(k)$ whenever $u_{\rm lq}(k) \notin \mathcal{U}$. The projection $P_{\mathcal{U}_b}(u_{b,{\rm lq}}(k))$ is computed by solving the following simple QP problem

$$\begin{aligned} &\text{minimize} \quad \|u_b(k) - u_{b,{\rm lq}}(k)\|^2 \\ &\text{subject to} \quad u_b(k) \in \mathcal{U}_b(k) \end{aligned} \quad \text{(P-III)}$$

where the time-varying set $\mathcal{U}_b(k)$ is defined in (20). The proposed control scheme is summarized as Algorithm 1.

Remark 1. Note that simply saturating the *total unconstrained control signal* $u_{\rm lq}$ cannot work as it does not respect the voltage constraint. The proposed method of handling constraint via projection of $u_{b,{\rm lq}}$ on $\mathcal{U}_b(k)$ can be considered as a special way of implementing saturation, which clips $u_{\rm lq}$ without violating the voltage constraint.

Algorithm 1 For Electrothermal Control of Battery

Data: Load demand $(v_{Ld}(k), i_L(k))$
for $k = 1$ to N_d **do**
  Compute $u_v(k)$ using (P-I)
  Compute $u_{b,{\rm lq}}(k)$ using (28)
  Compute $u_{\rm lq}(k)$ using (29)
  if $u_{\rm lq}(k) \notin \mathcal{U}$ **then**
    Compute $u_b(k) = P_{\mathcal{U}_b}(u_{b,{\rm lq}}(k))$ using (P-III)
  else
    $u_b(k) = u_{b,{\rm lq}}(k)$
  end if
  Compute $u(k) = u_v(k) + u_b(k)$
  Apply $u(k)$ to the modular battery system
end for

5. SIMULATION RESULTS AND DISCUSSION

The following simulation study is based on numerical solution of problems (P-I) and (P-III) and the analytical solution of control problem (P-II). To solve (P-I) and (P-III), we used `CVX`, a MATLAB-based package for specifying and solving convex programs using disciplined convex programming ruleset, see Boyd and Vandenberghe (2006) and Grant and Boyd (2011). The controller has been tuned using iterative trial and error method to achieve satisfactory balancing performance for various drive cycles with minimum possible prediction horizon N. The prediction horizon $N = 1$ gives satisfactory control performance in all cases. Note that for case $N = 1$, Riccati recursion is not needed and the control gain $K_{\rho_b}(k)$ is simply given by

$$K_{\rho_b}(k) = -[R_{\rho_b}(k) + \bar{B}_d^{\mathrm{T}}(k)\bar{P}_x\bar{B}_d(k)]^{-1}\bar{B}_d^{\mathrm{T}}(k)\bar{P}_x A_d. \quad (30)$$

where $\bar{P}_x$ is a fixed terminal penalty given by (24). The system has been discretized using Euler approximation with sampling interval $h = 1\,\mathrm{sec}$ and the coolant inlet temperature T_{f0} is assumed constant at 25°C.

5.1 Simulation Setup

The modular battery considered for this simulation study consists of 4 modules, each containing one cell ($3.3V$, $2.3Ah$, A123 ANR26650M1A). The nominal values of cell's electro-thermal parameters have been taken from Lin et al. (2013b). The cells are assumed to have capacity, SOC, and resistance variations as shown in Figure 2. The balancing performance under this parametric variation has been evaluated for various real world and certification drive cycles. However, due to space limitation, we present here results only for *Standard ARTEMIS Rural* drive cycle, which is representative of normal to intensive driving behavior. The battery load current data for ARTEMIS were obtained at 1 Hz by simulation of Toyota Prius PHEV in full EV mode in *Advisor* (Wipke et al. (1999)). The battery current (in c-rate) and its histogram are shown in Figure 3(b). The load voltage v_{Ld} demanded from battery is assumed as a constant dc-link voltage of a three-phase two-level inverter. It is chosen as $9.25\,V$ [1] for the case of four cell battery considered in this study.

Before presenting the simulation results, let us introduce

$$I_{Bai} = \frac{1}{N_d}\sum_{k=1}^{N_d} h \cdot i_{Bi}(k), \quad (31)$$

$$I_{Bri} = \sqrt{\frac{1}{N_d}\sum_{k=1}^{N_d} h \cdot i_{Bi}^2(k)}, \quad (32)$$

which are average and rms currents of each Cell_i respectively over a drive cycle of length N_d. These variables are used for illustrating control behavior in section 5.3.

[1] A certain level of surplus voltage (or cell redundancy) needed to achieve voltage regulation and balancing depends on a drive cycle. The voltage setting $v_{Ld} = 9.25\,V$ is used in Altaf et al. (2015) to ensure problem feasibility for three different drive cycles tested there. Although it is possible to choose higher voltage for ARTEMIS Rural drive cycle considered in this study, $9.25\,V$ is chosen for sake of compatibility and control comparison with Altaf et al. (2015).

5.2 Control Performance using One-step Prediction

The balancing performance of control Algorithm 1 with one-step ahead prediction ($N = 1$) has been thoroughly investigated. The simulation results are shown in Figure 3. The voltage regulation ($v_L(k) = v_{Ld}(k)$) is achieved despite large load variations as shown in Figure 3(c). In addition, the controller continuously reduces SOC imbalance throughout the driving and makes it negligible within 500 seconds as shown in Figure 3(d). The controller is also able to keep temperature deviations within almost 1°C limit during whole driving as shown in Figure 3(e), despite significant deviation among cell resistances and high c-rate loading. The unconstrained LQ control decisions and their projections (so-called *projected LQ control* decisions) on constraint set $\mathcal{U}_b(k) \in \mathbb{R}^4$ (whose projection on $\mathbb{R}^2$ is shown in Figure 3(a) for gridded $i_L \in \{-10c : 5c : 10c\}$) are shown in Figures 3(f) and 3(g) respectively. During initial period of high SOC imbalance, the unconstrained control policy demands quite aggressive actions, which violate the physical limits of the modular battery system, and are thus practically infeasible. The projected control actions are relatively mild, but are physically realizable to achieve promising balancing performance. It is also interesting to note that after initial aggressive balancing phase, the unconstrained LQ control actions are mostly within limits and the projections are needed only during high load current intervals.

5.3 Control Behavior

The projected duty cycles (control actions) of cells are shown in Figure 3(g). The imbalance among cell duties and the difference in control behavior for each cell is quite visible. In particular, the control behavior for cells 1 and 2 is much different from that for cells 3 and 4. The difference is necessary to achieve cell balancing in the presence of capacity and resistance variations. For example, cells 1 and 2, which have lower dischargeable capacities than cells 3 and 4, are used less relative to cells 3 and 4 during initial heavy SOC balancing phase. However, to avoid overheating of cells 3 and 4 during each time interval of high load current demand, the controller decreases the duties of cells 3 and 4, which have relatively higher resistances, and increases the duties of cells 1 and 2. Note the resemblance between duties of cells 1 and 2 and also between duties of cells 3 and 4 due to closely matched characteristics of two cells in each of these pairs.

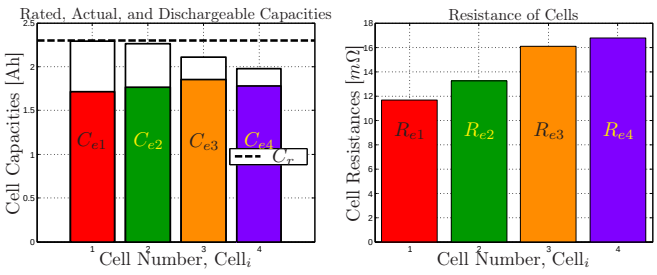

(a) Variation in cell capacities. (b) Variation in cell resistances.

Fig. 2. Figure shows capacity and resistance distribution of cells. Figure 2(a) shows variation in actual and dischargeable capacities, $C_{ed,i}(k) = \xi_i(k)C_{ei}$, along with rated capacity C_r of cells.

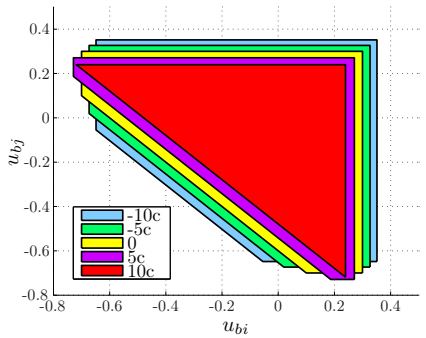

(a) Projection of set $\mathcal{U}_b(k) \subseteq \mathbb{R}^4$ on $\mathbb{R}^2$. Figure shows set variation as a function of i_L for a fixed voltage demand $v_{Ld} = 9.25\,V$.

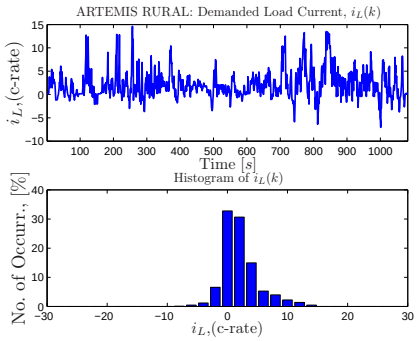

(b) Battery current and its histogram for Standard ARTEMIS Rural drive cycle.

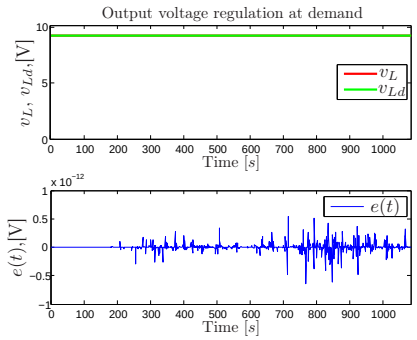

(c) Upper plot: voltage output of modular battery; lower plot: voltage error.

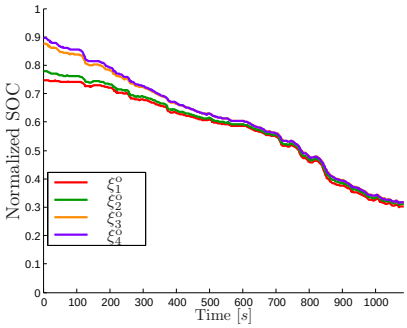

(d) SOC balancing performance.

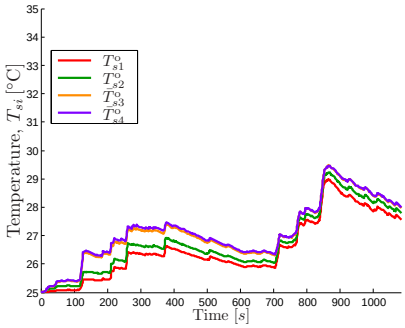

(e) Thermal balancing performance.

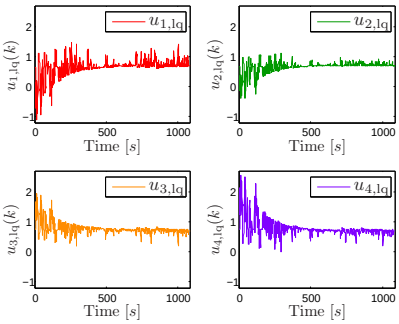

(f) Unconstrained LQ control signals.

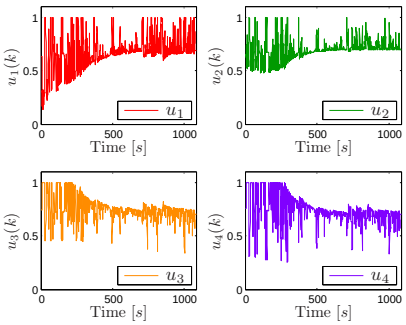

(g) Projected LQ Control Signals.

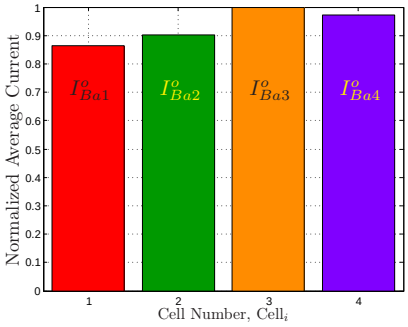

(h) Cell average currents under $u(k)$.

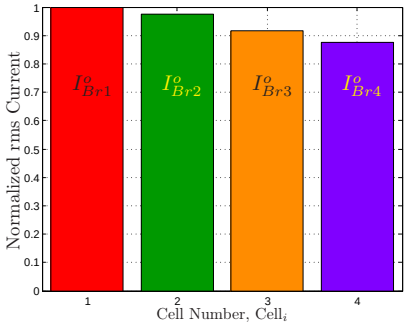

(i) Cell rms currents under $u(k)$.

Fig. 3. Simulation results of control Algorithm 1 using only one-step ahead prediction (one-step MPC). The figures show electro-thermal control performance under *ARTEMIS Rural* drive cycle.

To further understand the overall controller behavior, the distributions of average and rms currents among cells, under control trajectory $\{u(k)\}_{k=1}^{N_d}$ over whole drive cycle, are shown in Figures 3(h) and 3(i) respectively. It is interesting to note that the controller achieves thermal and SOC balancing by *redistributing* load among cells in such a way that their average current distribution resembles their dischargeable capacity distribution and their rms current distribution is the mirror image of their resistance distribution, compare Figure 3(h) with Figure 2(a) and Figure 3(i) with Figure 2(b). Because cells are not uniform in parameters, the uniform time-usage (so-called uniform duty cycle operation) of cells is not optimal. For example, if all cells in a string, with variations in dischargeable capacities, are equally loaded (same average current) then the cell with lower dischargeable capacity will be empty prior to other cells. Similarly, if all cells, with resistance variations, are equally loaded (same rms current) during whole drive cycle then a cell with higher resistance will naturally generate more heat, which will lead to higher temperature. See Altaf et al. (2013) and Altaf (2014) for performance comparison with uniform usage of cells.

6. SUMMARY AND CONCLUSIONS

The aim of this paper was to devise a simple predictive control scheme (i.e. based on several simpler subproblems instead of solving a single large problem) for thermal and SOC balancing as well as voltage regulation of a modular battery using limited future load information. For this purpose, we proposed a simple control algorithm based on LQ MPC scheme with orthogonal decomposition of controller into two components, one for voltage control (minimum norm problem) and the other for balancing control. The balancing controller is implemented in two stages. The first stage issues a *balancing control policy* by solving a

standard time-varying unconstrained LQ problem. The second stage generates *feasible control actions* ($u_i \in [0, 1]$) by projecting unconstrained LQ control signals on a time-varying control constraint polytope. The novel way of decomposing balancing task into two separate subtasks (i.e. first generating a control policy and then handling control constraint separately via projections) is one of the major contribution of this paper. This control algorithm, compared with control constrained LQ problem of Altaf et al. (2015), is not only easy to implement, but also easy to understand and interpret as it reveals more structure and properties of controller.

The performance of the proposed control algorithm has been thoroughly evaluated using one-step ahead prediction to assess its balancing potential for most realistic cases where no future load information is accessible. The results confirm the effectiveness of this simple scheme for benign to normal driving situations with short driving pulses as in ARTEMIS Rural drive cycle. The results revealed that only slight adjustments in cell duty cycles are needed to achieve promising balancing performance. Moreover, the unconstrained LQ controller is mostly sufficient (i.e. projections are rarely required) if the SOC imbalance and/or the load demand is not too high. The performance is quite encouraging for real-time control implementation in large battery packs. The proposed control scheme has special underlaying structure, which may also provide deeper insight into structural and functional properties of the balancer to implement even simpler controller in our future studies. We will also compare projected LQ problem of this paper with control-constrained LQ problem of Altaf et al. (2015) in our future work, where we will particularly try to establish equivalence between two control problems.

REFERENCES

Altaf, F., Egardt, B., and Johannesson, L. (2015). Load management of modular battery using model predictive control: Thermal and state-of-charge balancing. *IEEE Transactions on Control Systems Tech. (Submitted)*.

Altaf, F., Johannesson, L., and Egardt, B. (2014). Simultaneous thermal and state-of-charge balancing of batteries: A review. In *Vehicle Power and Propulsion Conference (VPPC), 2014 IEEE*.

Altaf, F., Johannesson, L., and Egardt, B. (2012). Evaluating the potential for cell balancing using a cascaded multi-level converter using convex optimization. In *IFAC Workshop on Engine and Powertrain Control, Simulation and Modeling, 2012*.

Altaf, F. (2014). *Thermal and State-of-Charge Balancing of Batteries using Multilevel Converters*. Licentiate Thesis, Chalmers University of Technology.

Altaf, F., Johannesson, L., and Egardt, B. (2013). On thermal and state-of-charge balancing using cascaded multi-level converters. *Journal of Power Electronics*, 13(4), 569–583.

Bandhauer, T.M., Garimella, S., and Fuller, T.F. (2011). A critical review of thermal issues in lithium-ion batteries. *Journal of the Electrochemical Society*, 158(3), R1–R25.

Barreras, J., Pinto, C., and et.al. (2014). Multi-objective control of balancing systems for li-ion battery packs: A paradigm shift ? In *Vehicle Power and Propulsion Conference (VPPC), 2014 IEEE*.

Boyd, S. and Vandenberghe, L. (2006). *Convex Optimization*. Cambridge University Press.

Cao, J., Schofield, N., and Emadi, A. (2008). Battery balancing methods: A comprehensive review. In *Vehicle Power and Propulsion Conference, 2008. VPPC '08. IEEE*, 1 –6.

Dubarry, M., Vuillaume, N., and Liaw, B.Y. (2010). Origins and accommodation of cell variations in li-ion battery pack modeling. *International Journal of Energy Research*, 34(2), 216–231.

Gallardo-Lozano, J., Romero-Cadaval, and et.el. (2014). Battery equalization active methods. *Journal of Power Sources*, 246, 934–949.

Grant, M. and Boyd, S. (2011). CVX: Matlab software for disciplined convex programming, version 1.21.

Groot, J. (2014). *State-of-Health Estimation of Li-ion Batteries: Ageing Models*. PhD Thesis. New Series, no: 3815. Chalmers University of Technology,.

Hu, X., Li, S., and Peng, H. (2012). A comparative study of equivalent circuit models for li-ion batteries. *Journal of Power Sources*, 198(0), 359 – 367.

Lin, X., Fu, H., Perez, H.E., and et.el. (2013a). Parameterization and observability analysis of scalable battery clusters for onboard thermal management. *Oil & Gas Science and Technology–Revue dŠIFP Energies nouvelles*, 68(1), 165–178.

Lin, X., Perez, H., Siegel, J., Stefanopoulou, A., and et.el. (2013b). Online parameterization of lumped thermal dynamics in cylindrical lithium ion batteries for core temperature estimation and health monitoring. *Control Systems Technology, IEEE Transactions on*, 21(5), 1745–1755.

Lu, L., Han, X., Li, J., Hua, J., and Ouyang, M. (2013). A review on the key issues for lithium-ion battery management in electric vehicles. *Journal of Power Sources*, 226, 272–288.

Mahamud, R. and Park, C. (2011). Reciprocating air flow for li-ion battery thermal management to improve temperature uniformity. *Journal of Power Sources*, 196(13), 5685 – 5696.

Malinowski, M., Gopakumar, K., Rodriguez, J., and Pérez, M. (2010). A survey on cascaded multilevel inverters. *Industrial Electronics, IEEE Transactions on*, 57(7), 2197 –2206.

Vetter, J., Novak, P., Wagner, M., and et.el. (2005). Ageing mechanisms in lithium-ion batteries. *Journal of power sources*, 147(1), 269–281.

Wang, J., Liu, P., Hicks-Garner, and et.el. (2011). Cycle-life model for graphite-$LiFePO_4$ cells. *Journal of Power Sources*, 196(8), 3942–3948.

Wipke, K., Cuddy, M., and Burch, S. (1999). Advisor 2.1: a user-friendly advanced powertrain simulation using a combined backward/forward approach. *Vehicular Technology, IEEE Transactions on*, 48(6), 1751–1761.